

Fig. 6.1 Viscosity of mixed-fluid as a function of particle volume fraction for gas-solid flows at: a) high-frequency limit, b) low frequency limit.

a)

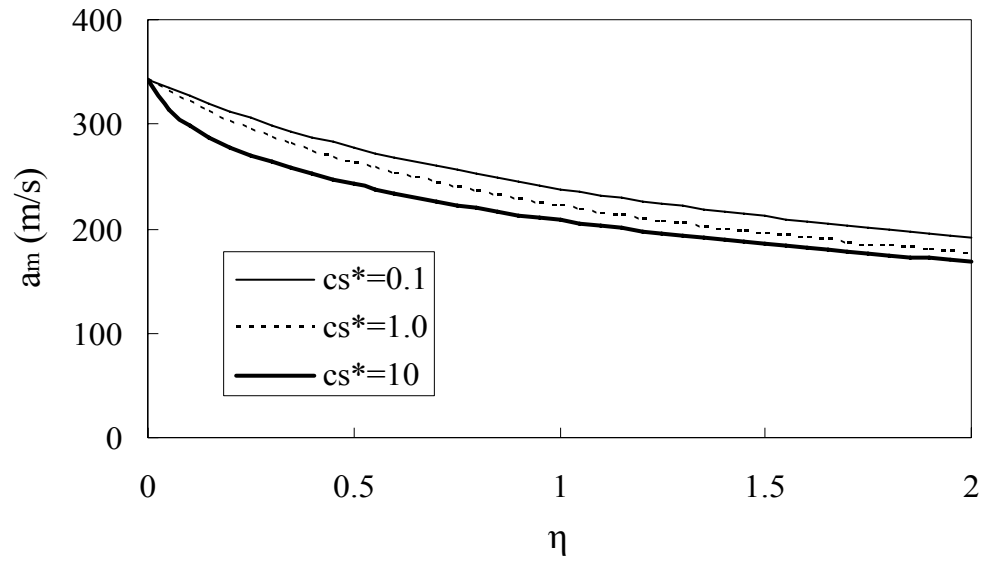


Fig. 6.2 Speed of sound of a dusty gas as a function of mass loading and specific heat ratio based on ideal-gas theory.

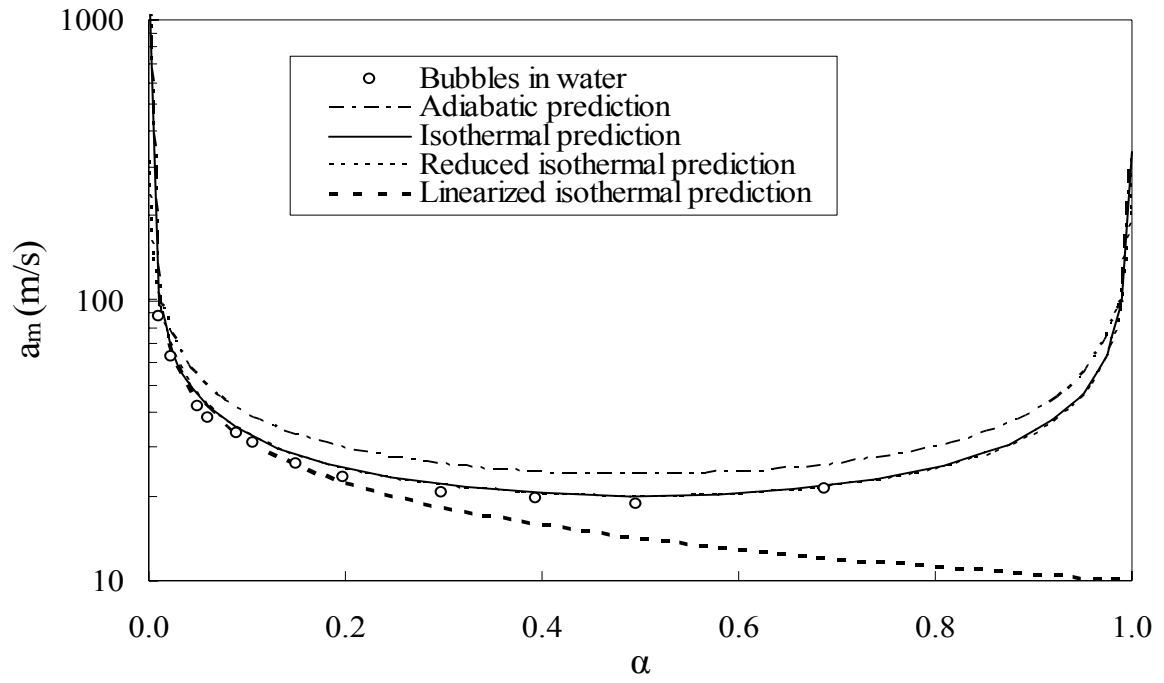


Fig. 6.3 Speed of sound of mixed-fluid for bubbles in water at low frequencies.

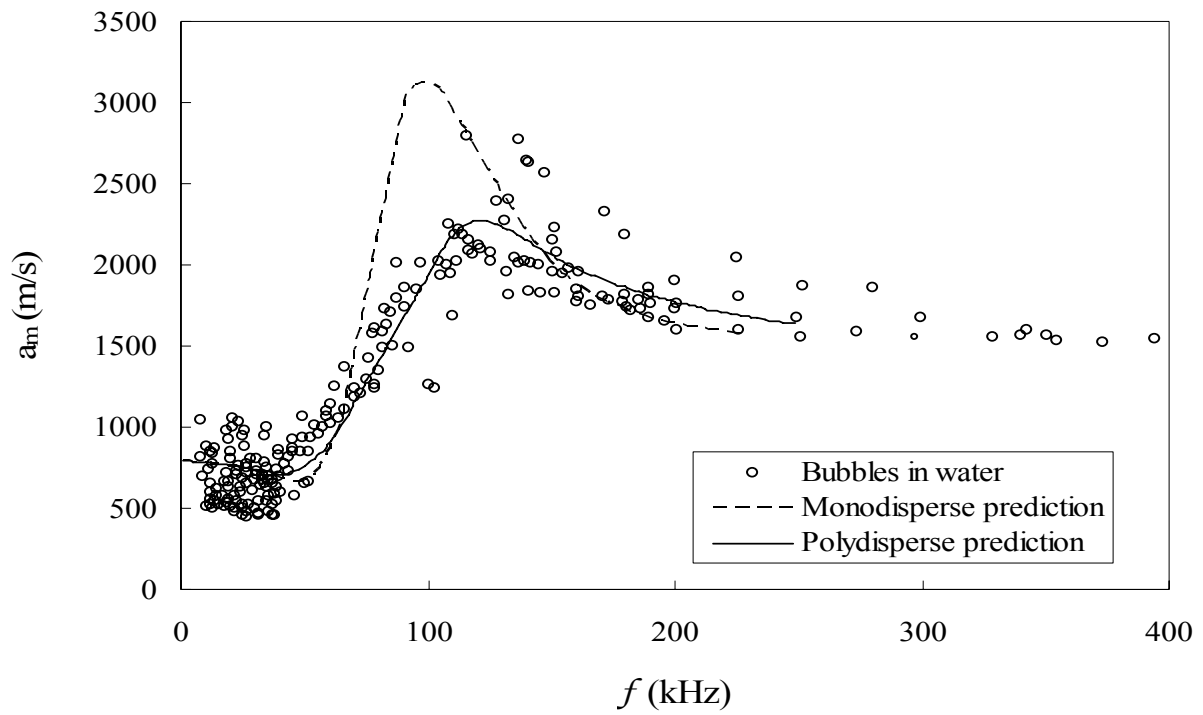


Fig. 6.4X Speed of sound of mixed-fluid for bubbles in water as a function of frequency for a mean bubble diameter of  $220\mu\text{m}$  and  $\alpha = 0.0002$  (Brennen, 2005).

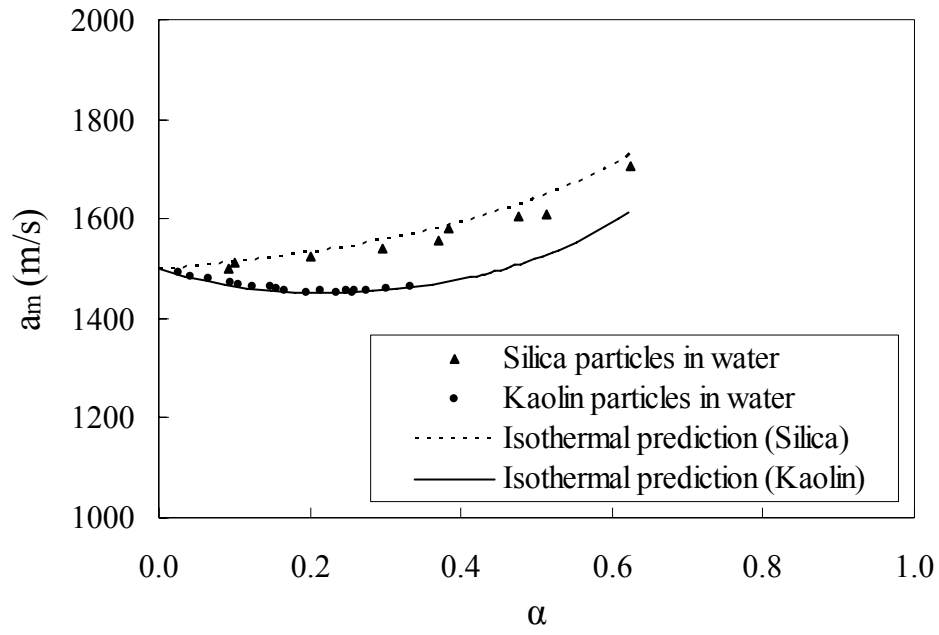
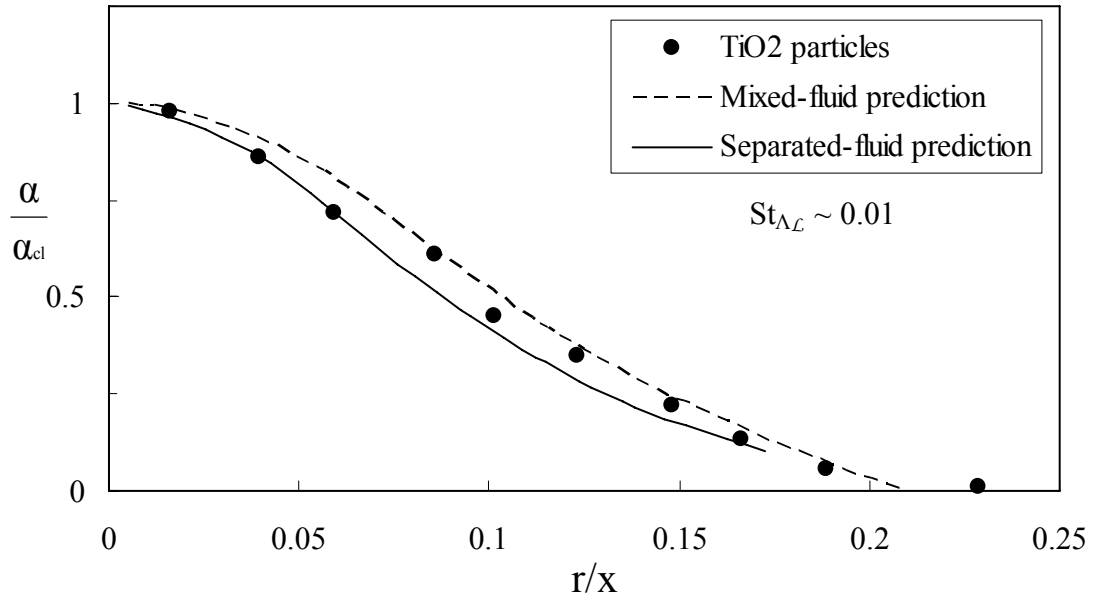


Fig. 6.4 Theoretical and experimental speed of sound of 0.5 $\mu$ m solid particles in water as a function of volume fraction for low frequency (Brennen, 2005).

$\mathbf{q}$	$\mathbf{c}_q$	$\mathcal{S}_q$
1	-	0
$\tilde{X}_p$	0.7	0
$\tilde{u}_{m,i}$	1.0	$\tilde{\alpha}(\rho_\infty - \bar{\rho}_m) g_i$
$k_m$	1.0	$\mu_{m,turb} \left( \frac{\partial \tilde{u}_{m,x}}{\partial r} \right)^2 - \bar{\rho} \epsilon_m$
$\epsilon_m$	1.3	$1.44 \mu_{m,turb} \left( \frac{\epsilon_m}{k_m} \right) \left( \frac{\partial \tilde{u}_{m,x}}{\partial r} \right)^2 - 1.9 \bar{\rho}_m \left( \frac{\epsilon_m}{k_m} \right)$

Table 6.1 Axi-symmetric mixed-fluid transport.

a)



b)

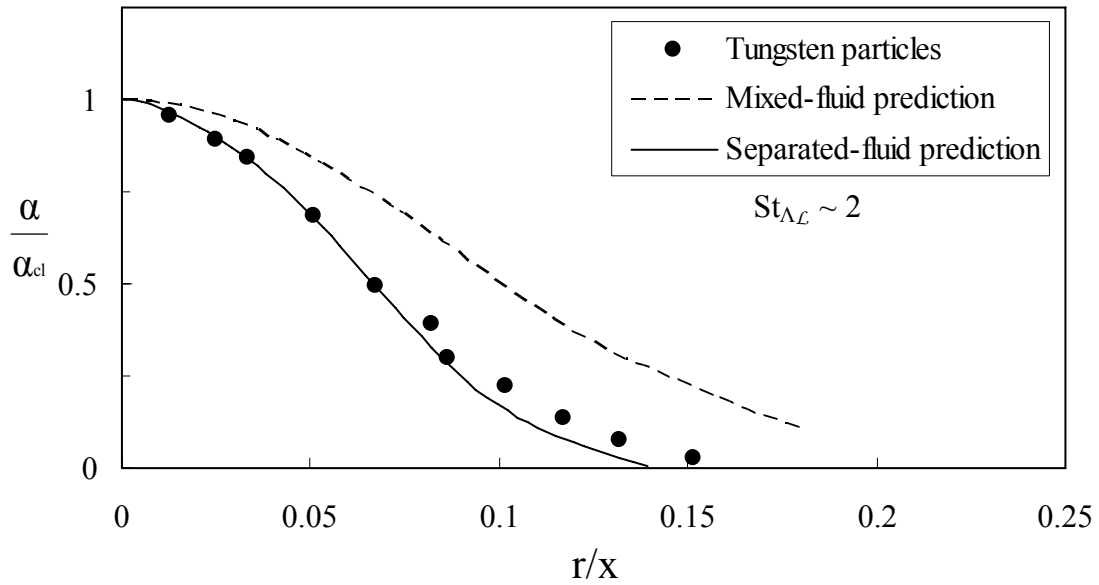


Fig. 6.5 Normalized volume concentration in particle-laden round gas jets of McComb and Salih (1977, 1978) compared to mixed-fluid and separated-fluid predictions (Faeth, 1987) for: a) titanium dioxide particles and b) tungsten particles.

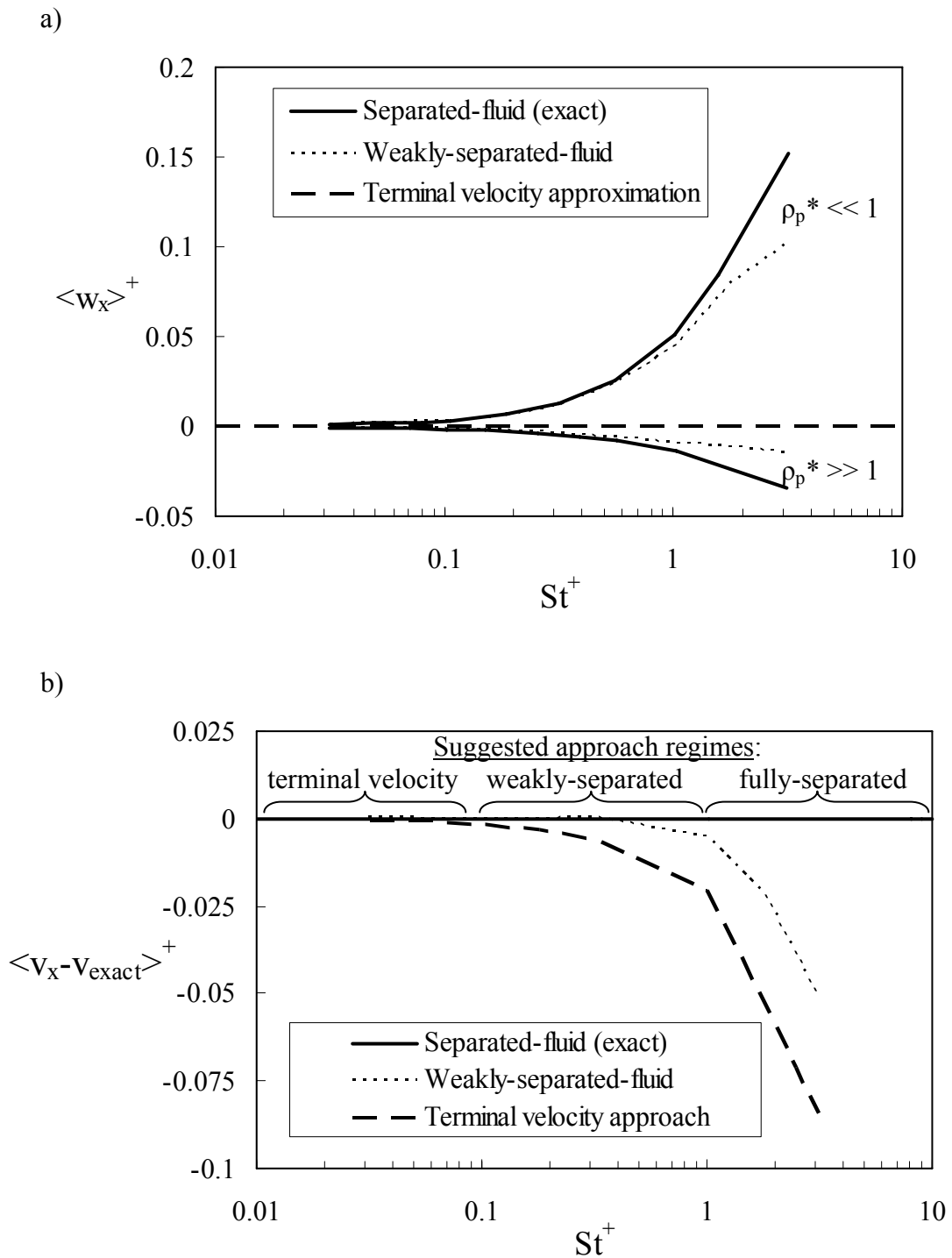


Fig. 6.6 Comparison of ensemble-averaged prediction at  $y^+=20$  for particles in a turbulent channel flow: a) predicted streamwise relative velocity bias results for both high-density and very-buoyant particles b) streamwise particle velocity for  $\rho_p^* \gg 1$  with suggested Stokes number ranges for various approaches (Ferry and Balachandar, 2001).